Young's double-slit experiment using core-level photoemission from N_2: revisiting Cohen–Fano's two-centre interference phenomenon

2006 J. Phys. B: At. Mol. Opt. Phys. 39 4801

(http://iopscience.iop.org/0953-4075/39/23/001)

INSTITUTE OF PHYSICS PUBLISHING JOURNAL OF PHYSICS B: ATOMIC, MOLECULAR AND OPTICAL PHYSICS

J. Phys. B: At. Mol. Opt. Phys. **39** (2006) 4801–4817 doi:10.1088/0953-4075/39/23/001

Young's double-slit experiment using core-level photoemission from N_2: revisiting Cohen–Fano's two-centre interference phenomenon

X-J Liu[1], N A Cherepkov[1,2], S K Semenov[2], V Kimberg[3], F Gel'mukhanov[1,3,5], G Prümper[1], T Lischke[1], T Tanaka[4], M Hoshino[4], H Tanaka[4] and K Ueda[1]

[1] Institute of Multidisciplinary Research for Advanced Materials, Tohoku University, Sendai 980-8577, Japan
[2] State University of Aerospace Instrumentation, 190000, St. Petersburg, Russia
[3] School of Biotechnology, Royal Institute of Technology, S-106 91 Stockholm, Sweden
[4] Department of Physics, Sophia University, Tokyo 102-8554, Japan

E-mail: ueda@tagen.tohoku.ac.jp

Received 13 July 2006, in final form 19 September 2006
Published 10 November 2006
Online at stacks.iop.org/JPhysB/39/4801

Abstract

The core-level photoelectron spectra of N_2 molecules are observed at high energy resolution, resolving the $1\sigma_g$ and $1\sigma_u$ components as well as the vibrational components in the extended energy region from the threshold up to 1 keV. The σ_g/σ_u cross section ratios display modulation as a function of photoelectron momentum due to the two-centre interference, analogous to the classical Young's double-slit experiment, as predicted by Cohen and Fano a long time ago. The Cohen–Fano interference modulations display different phases depending on the vibrational excitations in the core-ionized state. Extensive *ab initio* calculations have been performed within the Hartree–Fock and random phase approximations in prolate spheroidal coordinates. The dependence of photoionization amplitudes on the vibrational states was taken into account using the Born–Oppenheimer approximation. The *ab initio* results are in reasonable agreement with the experimental data. The theoretical analysis allows the modulation to be connected with the onset of transitions to the states of increasing orbital angular momentum which occurs at increasing photon energies. Deviation from the Cohen–Fano formula is found for both the experimental and the *ab initio* results and is attributed to electron scattering by the neighbouring atom. A new formula for the interference modulation is derived within the framework of the multiple scattering technique. It differs from the classical Cohen–Fano formula by the addition of twice the scattering phase of the photoelectron by the neighbouring atom. We demonstrate that

[5] Permanent address: Institute of Automation and Electrometry 630090 Novosibirsk, Russia.

one can measure directly the scattering phase by fitting our formula to the experimental results.

(Some figures in this article are in colour only in the electronic version)

1. Introduction

The Young's double-slit experiment (YDSE) provides the simplest and most fundamental example in which the addition of two coherent waves of light leads to interference oscillations of the light intensity. Photoionization of diatomic molecules represents conceptually a similar phenomenon for the electron waves. Instead of passing through the holes in a screen the photoelectron is ejected from an orbital described as a linear combination of two atomic orbitals (LCAO) localized in different atoms. The interference of the coherent electron waves emitted from two indistinguishable atoms leads to intrinsic interference oscillations similar to YDSE. Cohen and Fano [1] were the first to derive the equation for the total photoionization cross section for the H_2 molecule including this YDSE effect. Stimulated by this pioneering work, some theoretical [2–5] and experimental [6–8] studies of ionization of H_2 and D_2 molecules with different projectiles were performed. Results of these experiments clearly exhibited the Cohen–Fano (CF) interference modulation.

Core-level photoemission from molecules like N_2 provides a new opportunity to investigate coherent emission of photoelectron waves (see, for example, [9]). For core-level photoionization of these molecules, an additional complication appears due to the presence of the gerade and ungerade 1σ bound orbitals with a very small energy gap between them. This gap is 0.1 eV and is even smaller than the vibrational splitting of ∼0.3 eV. Modern high-resolution x-ray photoelectron spectroscopy using synchrotron radiation as a light source is, however, able to resolve this small splitting [10–12]. This opens the possibility of performing YDSE using core-level photoionization of N_2 and observing the CF interference modulation, as briefly discussed in our preliminary report [13]. In this paper, we present our extensive investigations, both experimental and theoretical, for the CF interference modulation in the core-level photoemission of the N_2 molecule. The present theoretical analysis of the CF interference modulation elucidates the physics of the intramolecular photoelectron scattering and provides a new tool to determine the electron phase shift due to the scattering by the neighbouring atom from the displacement of the interference modulation.

The paper is organized as follows. In section 2, we describe the high-resolution measurements of core-level photoelectron spectra of the N_2 molecule in the extended energy region from the threshold up to 1 keV. The unprecedented resolutions achieved for both the soft x-ray monochromator and electron energy analyser make this challenging experiment possible. We show that the measured σ_g/σ_u cross section ratios for vibrational transitions $v = 0 \rightarrow v' = 0$ and $v = 0 \rightarrow v' = 1$ modulate as a function of the photoelectron momentum. This modulation is caused by the two-centre interference, which is analogous to the interference modulations seen in the classical Young's double-slit experiment, as predicted by Cohen and Fano (CF) [1] in 1966. Sections 3 and 4 present our theoretical analysis. In section 3, we describe our *ab initio* calculations within the random phase approximations (RPA) with the use of the relaxed core Hartree–Fock (RCHF) wavefunctions as a zero-order approximation. We will show that the *ab initio* calculations are in reasonable agreement with the experiments. We then demonstrate that the modulation is connected with the behaviour of the partial cross sections corresponding to different angular momenta of the photoelectron

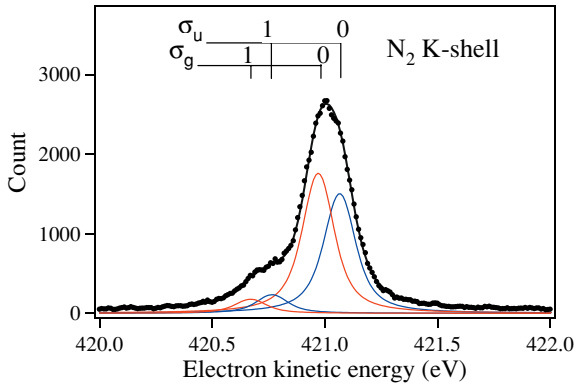

Figure 1. Photoelectron spectrum at photon energy of 831 eV, parallel to the polarization vector. Circles—experiment; thick solid line—fitted spectrum; thin lines—individual peaks.

wavefunction. The onsets of these contributions with increasing angular momentum are shifted to higher and higher energies. Summation over all partial waves leads to the appearance of the modulation of the cross section. In section 4, we focus on the high energy region. To give insights into the physics, we investigate the high energy asymptotic of the wavefunction of the fast photoelectron. We first briefly review the CF treatment [1] and demonstrate a deviation of both experimental and *ab initio* results from the classical CF formula. The deviation is attributed to electron scattering by the neighbouring atom, which is neglected in the CF model. A new formula for the interference modulation is derived within the framework of the multiple scattering technique. It differs from the classical CF formula by the addition of twice the scattering phase of the photoelectron by the neighbouring atom. We demonstrate that one can measure directly the scattering phase by fitting our formula to the experimental results. Section 5 presents our concluding remarks.

2. Experimental details

The experimental set-up, experimental procedure and data analysis were similar to those described elsewhere [11–14]. Briefly, the experiment was carried out at the high-resolution soft x-ray photochemistry beam line 27SU [15, 16] at SPring-8, Japan. The light source of the beam line is a figure-8 undulator [17] which provides linearly polarized radiation, whose polarization axis can be selected either horizontal or vertical by changing just the undulator gap, without changing any other optics. In the present high energy measurement, only horizontally polarized radiation was used. The heart of the electron spectroscopy apparatus is a 20 cm radius hemispherical electron energy analyser (Gammadata-Scienta SES-2002) [18]. The lens axis of the analyser is set in the horizontal direction. In the present experiment, the analyser bandwidth was set to ∼31 meV. The overall bandwidth, i.e., a convolution of the monochromator and analyser bandwidths, was determined separately by measuring Xe 5p photoelectrons at the same monochromator and analyser settings.

Figure 1 shows an example of the N 1s photoelectron spectrum recorded at a photon energy of 831 eV. The experimental spectra recorded at different energies up to ∼1 keV have been decomposed by least-squares curve fitting into $1\sigma_g$ and $1\sigma_u$ components with the individual vibrational progressions, as seen in figure 1. The Lorentzian widths were fixed to the values previously determined; 120 meV for both $1\sigma_g$ and $1\sigma_u$ [13]. The Gaussian widths were fixed

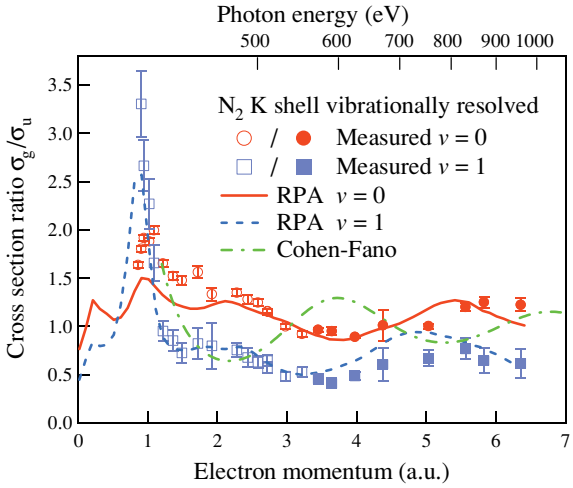

Figure 2. Comparison of experimental cross section ratios with *ab initio* calculations. Open and full symbols: previous [11–13] and present experiments, respectively.

to the values obtained from the separate measurements. The $1\sigma_g$–$1\sigma_u$ splitting of the $v' = 1$ vibrational components was 97 meV [12]. The vibrational spacings were also fixed to 298 meV for $1\sigma_g$ and 300 meV for $1\sigma_u$ [12]. The position of the $1\sigma_u$ $v' = 0$ component and the intensities of the individual vibrational components were treated as fitting parameters. The partial cross section ratios of σ_g/σ_u for the photoionization of the $1\sigma_g$ and $1\sigma_u$ shells corresponding to the $0 \rightarrow 0$ and $0 \rightarrow 1$ vibrational transitions are extracted from the fitting and are plotted in figure 2 as a function of the photoelectron momentum $k = \sqrt{2E}$, with E being the kinetic energy of the photoelectron in atomic units. (Atomic units are used throughout the paper unless otherwise indicated.) The results of previous measurements [11–13] are also included in the figure. The peak structure appears at $k \simeq 1$ au. It corresponds to the σ^* shape resonance as discussed in detail in [11]. In the region of $1.5 < k < 6.5$ au, the ratios exhibit the oscillatory structure. This oscillatory structure is the CF interference pattern.

3. Ab initio calculations

3.1. Methodology

The accurate calculation of the photoionization cross section in the extended photon energy region has been performed using the RPA method developed earlier in [19, 20] for diatomic molecules. As usual, it is implied that the Born–Oppenheimer approximation is valid. As the first step, the Hartree–Fock ground and excited state wavefunctions of a diatomic molecule are calculated from the self-consistent equations

$$\left[-\frac{\nabla^2}{2} - \frac{Z_1}{r_1} - \frac{Z_2}{r_2} + \sum_{j=1}^{n} a_{ij} J_{jj}(\mathbf{r})\right] \varphi_i(\mathbf{r}) - \sum_{j=1}^{n} b_{ij} J_{ji}(\mathbf{r}) \varphi_j(\mathbf{r})$$
$$= \epsilon_i \varphi_i(\mathbf{r}) + \sum_{j=1}^{n} \epsilon_{ij} \varphi_j(\mathbf{r}), \qquad i \leqslant n, \tag{1}$$

where n is the number of occupied orbitals. The functions $J_{ji}(\mathbf{r})$ are defined as the integrals

$$J_{ji}(\mathbf{r}) \equiv J[\varphi_j(\mathbf{r}), \varphi_i(\mathbf{r})] = \int \varphi_j^*(\mathbf{r}')|\mathbf{r} - \mathbf{r}'|^{-1}\varphi_i(\mathbf{r}')\,\mathrm{d}\mathbf{r}'. \tag{2}$$

They describe the exchange interaction when $i \neq j$ and the direct interaction when $i = j$. The values of off-diagonal energy parameters ϵ_{ij} are determined from the orthogonalization condition

$$\int \varphi_j^*(\mathbf{r})\varphi_i(\mathbf{r})\,\mathrm{d}\mathbf{r} = 0. \tag{3}$$

Below we consider only the case of closed-shell molecules. Then system (1)–(3) is solved with the coefficients $a_{ij} = 2$, $b_{ij} = 1$ to find a usual set $\varphi_i(\mathbf{r})$ of the ground state wavefunctions. For the excited state wavefunctions of the discrete and continuous spectrum, several procedures have been proposed. One of them corresponds to the frozen core HF (FCHF) approximation in which the photoelectron is moving in the field of a singly charged ion constructed from the ground state wavefunctions with one electron absent from the ionized shell. Another possibility corresponds to the relaxed core HF (RCHF) approximation [21] in which the photoelectron wavefunction is calculated in the field of a singly charged ion obtained by solving the self-consistent HF equations for the ion. From numerous calculations it is known that the relaxation effect is important, but on the other hand the RCHF approximation overestimates the relaxation effect. Therefore it was proposed in [22] to use the fractional charge RCHF approximation in which system (1)–(3) is solved with the coefficients expressed through the fractional parameter z_e $(0 < z_e < 1)$,

$$\begin{aligned} &a_{i'i'} = 2(1 - z_e), && b_{i'i'} = 1 - z_e, && \\ &a_{ii'} = 2 - z_e, && b_{ii'} = 0.5(2 - z_e), && i \neq i', \\ &a_{i'j} = 2, && b_{i'j} = 1, && j \neq i', \end{aligned} \tag{4}$$

to determine a set of relaxed core HF wavefunctions $\varphi_i^R(\mathbf{r})$. We consider z_e as a free parameter which is found from the condition to reproduce correctly the experimental data. The FCHF approximation corresponds to $z_e = 0$, while the standard RCHF method [21] corresponds to $z_e = 1$. In this paper we accepted $z_e = 0.7$, which gives a correct position of the σ^* shape resonance [11]. The excited state wavefunctions are found as solutions of the following equation,

$$\left[-\frac{\nabla^2}{2} - \frac{Z_1}{r_1} - \frac{Z_2}{r_2} + \sum_{j=1}^{n} a_{fj} J_{jj}^R(\mathbf{r})\right]\varphi_f(\mathbf{r}) - \sum_{j=1}^{n} b_{fj} J_{fj}^R(\mathbf{r})\varphi_j^R(\mathbf{r})$$
$$= \varepsilon_f \varphi_f(\mathbf{r}) + \sum_{j=1}^{n} \varepsilon_{fj}\varphi_j(\mathbf{r}), \tag{5}$$

where $f > n$, $J_{jj}^R(\mathbf{r}) \equiv J\left[\varphi_j^R(\mathbf{r}), \varphi_j^R(\mathbf{r})\right]$, $J_{fj}^R(\mathbf{r}) \equiv J\left[\varphi_f(\mathbf{r}), \varphi_j^R(\mathbf{r})\right]$,

$$a_{fj} = 2, \qquad b_{fj} = 1, \qquad j \neq i'; \qquad a_{fi'} = 1, \qquad b_{fi'} = -1. \tag{6}$$

Index i' corresponds to the ionized shell. The off-diagonal energy parameters provide the orthogonalization of the excited state wavefunction to the ground state wavefunctions,

$$\int \varphi_f^*(\mathbf{r})\varphi_i(\mathbf{r})\,\mathrm{d}\mathbf{r} = 0. \tag{7}$$

The fractional charge in our method is used only in calculating the wavefunctions which create the Hartree–Fock potential in equation (5).

The photoionization parameters are defined using the photoelectron orbital $\psi_{\mathbf{k}}^{(-)}(\mathbf{r})$ with the incoming-wave boundary condition. Here $\mathbf{k}$ is the electron momentum and $\mathbf{r}$ is its

coordinate. The partial wave expansion of this orbital in the molecular frame is given as usual [23, 22] by

$$\psi_{\mathbf{k}}^{(-)}(\mathbf{r}) = \sum_{lm} (i)^l \, f_{\varepsilon lm}(\mathbf{r}) Y_{lm}^*(\Omega_k), \tag{8}$$

where $\varepsilon = k^2/2$ is the photoelectron energy, Ω_k denotes the spherical angles of vector $\mathbf{k}$, functions $f_{\varepsilon lm}(\mathbf{r})$ satisfy equation (5) and have the asymptotic

$$f_{\varepsilon lm}(\mathbf{r})|_{r\to\infty} \sim \left(\frac{2}{\pi k}\right)^{1/2} \frac{1}{2\mathrm{i}r} \left(Y_{lm}(\Omega_r)\, \mathrm{e}^{\mathrm{i}\vartheta(r)} + \sum_{l'} Y_{l'm}(\Omega_r) S_{ll'm}^* \, \mathrm{e}^{-\mathrm{i}\vartheta(r)} \right) \tag{9}$$

with $\vartheta(r) = kr + k^{-1} \ln 2kr - \pi l/2$. They are normalized to the energy δ-function. Within the Born–Oppenheimer approximation the partial photoionization cross section is presented as

$$\sigma(\omega) = \sum_{l,m} \sigma_{lm}(\omega) = \frac{4}{3}\pi^2 \alpha a_0^2 \omega \sum_{l,m} \sum_{\mu} |\langle f_{\epsilon lm}(\mathbf{r}) | d_\mu | i \rangle|^2. \tag{10}$$

Here ω is the photon energy, α is the fine structure constant, a_0 is the Bohr radius, $|i\rangle$ means the initial (ground) state of the molecule, and d_μ are the spherical projections of the dipole operator

$$d_\mu = \sqrt{4\pi/3} r Y_{1\mu}(\Omega_r). \tag{11}$$

The rotational motion is here neglected. The method of calculation of the continuum wavefunctions $f_{\varepsilon lm}$ has been described earlier [19]. It is worth noting that the cross section in equation (10) is the one averaged over molecular orientations and integrated over the direction of the photoelectron emission.

As the next step, we are looking for the dipole matrix elements in the RPA by solving the corresponding RPA equation, without calculating explicitly the wavefunctions in the RPA [24, 19].

To take into account the vibrational motion, the calculations described above have been performed for several fixed internuclear distances R giving a set of dipole matrix elements $d_{lm}(\omega, R) \equiv \langle f_{\epsilon lm}(\mathbf{r}) \, | d_m | \, i \rangle$ for each photon energy ω. To obtain the matrix element for vibrationally resolved transition, $d_{lm}(\omega, v, v')$, the values $d_{lm}(\omega, R)$ were multiplied by the corresponding initial and final vibrational state wavefunctions, $\chi_v^{(i)}(R)$ and $\chi_{v'}^{(f)}(R)$, and integrated over the internuclear distance R,

$$d_{lm}(\omega, v, v') = \int \chi_{v'}^{(f)}(R) d_{lm}(\omega, R) \chi_v^{(i)}(R) \, \mathrm{d}R. \tag{12}$$

We used the Morse potential vibrational wavefunctions (see [25] for details) in the same way as was done in [26]. Assuming that in the initial state only the ground vibrational level $v = 0$ is populated, we integrated over R using nine points around the equilibrium distance $R = 2.068$ au of the ground state with step 0.05 au. The equilibrium internuclear distances for the $1\sigma_\mathrm{g}$ and $1\sigma_\mathrm{u}$ molecular ion states and the anharmonicity constants of the Morse potential were taken from [27].

3.2. Comparison with experiments

In general, the interference modulation is expected to be relatively small. The effect is stronger for the ratio of the photoionization cross sections of the gerade and ungerade core levels (see the discussion below). Therefore figure 2 shows the ratios of the cross sections for the $v = 0 \to v' = 0$ and $v = 0 \to v' = 1$ vibrational transitions measured experimentally

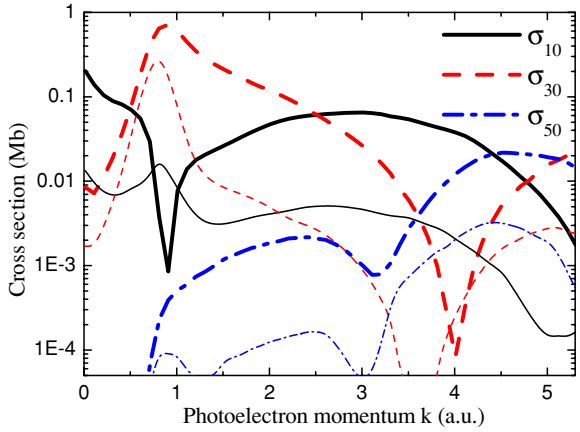

Figure 3. The partial photoionization cross sections $\sigma_{l,\lambda}$ of the $1\sigma_g \rightarrow \varepsilon\sigma_u$ transitions for three partial waves $l = 1, 3, 5$ and $\lambda = 0$ for the first two vibrational transitions $0 \rightarrow 0$ (thick lines) and $0 \rightarrow 1$ (thin lines) calculated in the RPA.

and calculated in the RPA. It should be noted that the experimental ratios for the photon energies above 460 eV were obtained for electron emission parallel to the electric vector while the theoretical results are those after integrating over the direction of the electron emission. However, the calculated values of the anisotropy parameters β are close to the limiting value 2 in the high energy region and thus the present comparison is verified. The ratios are shown as a function of the photoelectron momentum k in order to display clearly the oscillations. At low momenta $k < 1.5$ au the ratios are defined by the σ^* shape resonance, and only at $k > 1.5$ au the CF oscillations become apparent. There is a good qualitative agreement between our theory and the experiment for both vibrational transitions. The theoretical maxima in the σ^* shape resonance (at the photoelectron momentum 0.9 au) are lower than the experimentally observed ones. This is connected with some overestimation of the magnitude of the correlationally induced maximum in the $1\sigma_u$ partial cross section in the RPA as was discussed in [11].

The measured interference modulations of the ratios σ_g/σ_u for the $0 \rightarrow 0$ and $0 \rightarrow 1$ vibrational transitions approximately coincide in phase, but the oscillations are about different average values. This is explained by the difference between the Franck–Condon factors for the $0 \rightarrow 1$ and $0 \rightarrow 0$ transitions for the $1\sigma_g$ and $1\sigma_u$ shells, respectively. The corresponding ratio of the Franck–Condon factors for the $1\sigma_g$ shell is substantially smaller than for the $1\sigma_u$ shell (see figure 5 in [11]).

3.3. Origin of the interference modulation

The RPA calculation gives the possibility of studying the origin of the interference modulation. Since the vibrationally resolved calculations are time consuming, for a qualitative understanding of the phenomenon it is sufficient to study the cross sections without vibrational resolution obtained at the equilibrium internuclear distance. We also checked that the role of many-electron correlations at high energies is small; therefore in many cases we restricted our calculations by the RCHF approximation for $k > 3$ au. Vibrationally unresolved partial cross sections for the $1\sigma_g \rightarrow \varepsilon l\sigma_u$ and $1\sigma_g \rightarrow \varepsilon l\pi_u$ transitions for different partial waves up to $l = 11$ have been already presented in figure 2 of [13]. To demonstrate how the vibrational motion influences the interference modulation we show in figure 3 the partial cross

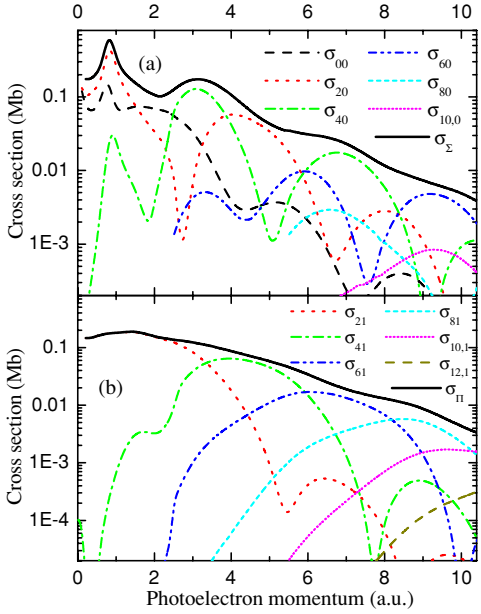

Figure 4. The partial photoionization cross sections $\sigma_{l,\lambda}$ of the $1\sigma_u \to \varepsilon l\sigma_g$ (a) and $1\sigma_u \to \varepsilon l\pi_g$ (b) transitions for different partial waves up to $l = 12$ calculated in the RPA (at $k \leqslant 3$ au) and the RCHF (at $k > 3$ au) approximation. The corresponding sums of all partial waves, σ_Σ and σ_Π are also shown.

sections $\sigma_{l,\lambda}$ for the $1\sigma_g \to \varepsilon l\sigma_u$ transitions for the first three partial waves $l = 1, 3, 5$ and for the first two vibrational transitions $0 \to 0$ and $0 \to 1$. The $0 \to 0$ transitions give a predominant contribution to the cross section, and the corresponding results are rather close to the vibrationally unresolved data published in [13]. This proves that for a qualitative study of the interference modulation one can restrict consideration by the vibrationally unresolved calculation. The partial cross sections for the $0 \to 1$ transitions behave similarly to the corresponding $0 \to 0$ transitions but are about one order of magnitude smaller and modulations are shifted somewhat to lower momenta. This shift is different for different partial waves.

In figure 4 we show the cross sections for the $1\sigma_u \to \varepsilon l\sigma_g$ and $1\sigma_u \to \varepsilon l\pi_g$ transitions for different partial waves up to $l = 12$. The total cross sections for the σ and π channels, σ_Σ and σ_Π, are also shown there. Like the $1\sigma_g$ case (see [13]) these figures demonstrate that the interference modulation is connected mainly with the onset of transitions to the states of increasing orbital angular momentum at increasing photon energies. This was mentioned already in the pioneering work of Cohen and Fano [1]. However, in reality the picture is more complicated due to the existence of Cooper-like minima in every partial cross section. Let us consider the σ channels in more detail. At $k \cong 0.9$ au in the σ channels with $l = 0, 2, 4$ there are the correlational maxima appearing due to the channel interaction between the $\sigma \to \sigma$ transitions of the $1\sigma_g$ and $1\sigma_u$ shells [11, 20]. The next two maxima in figure 4(a) at $k \cong 3.1$ au and $k \cong 6.8$ au are formed mainly by two consecutive maxima of the $l = 4$ partial wave. The last maximum shown in the figure at $k \cong 10$ au is formed by the $l = 6$ partial contribution. The maxima of the $l = 0$ and $l = 2$ partial contributions at these momenta are basically filling the minima of the $l = 4$ partial contribution and do not give any visible maxima in

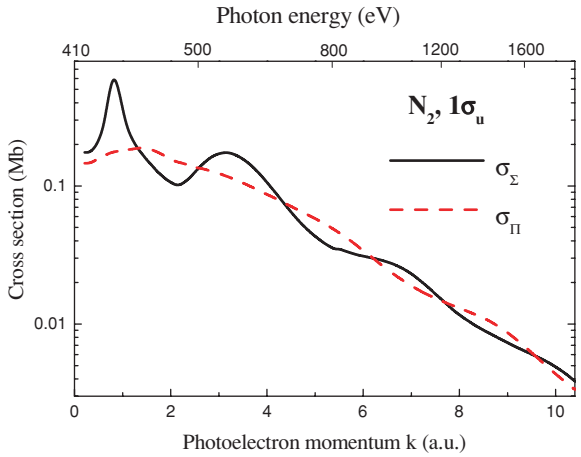

Figure 5. The cross sections σ_Σ and σ_Π for the $1\sigma_u$ shell.

the total cross section σ_Σ. For the $1\sigma_u \rightarrow \varepsilon l\pi_g$ transitions (see figure 4(b)) the situation is simpler because the maxima after the first Cooper-like minima are too small to give an important contribution and the interference modulation is more directly related to the onset of contributions of different partial waves. However, even in this case there is no simple correspondence between the sequential interference maxima and the sequential onsets. In particular, the consecutive maxima at $k \cong 1.4$, 5 and 9 au are formed mainly by the onset of the $l = 2, l = 4$ and $l = 8$ partial waves, respectively, while the onset of the $l = 6$ partial wave does not produce a maximum.

It is important to note that the interference modulation of the σ_Π cross section is much smaller in magnitude as compared to the modulation of the σ_Σ cross section and is in antiphase with it. This is illustrated in figure 5 for the $1\sigma_u$ shell. As a result, the modulation of the total cross section for the $1\sigma_u$ shell (that is, $\sigma_\Sigma + 2\sigma_\Pi$) coincides in phase with the modulation of the σ_Σ cross section and is smaller in magnitude (see figure 7).

The main difference between the $1\sigma_g$ and $1\sigma_u$ shells is connected with the symmetry of these states. From the dipole selection rules it follows that only odd partial waves contribute to the photoionization of the $1\sigma_g$ shell, and only even partial waves to the $1\sigma_u$ shell. Since the interference modulation is mainly connected with the onset of transitions to the states of increasing orbital angular momentum l at increasing photon energies, the different parity of the photoelectron partial waves for the $1\sigma_g$ and $1\sigma_u$ shells causes the shift of interference modulation for these shells by π. In other words, the interference modulations for the $1\sigma_g$ and $1\sigma_u$ shells are in antiphase as illustrated in figure 6 for the corresponding σ_Σ cross sections. Due to this, the cross section ratio $1\sigma_g/1\sigma_u$ observed experimentally and shown in figure 2 is greatly enhanced. Similar CF oscillations have been discovered earlier in the non-dipole parameters for the $1\sigma_g$ and $1\sigma_u$ shells characterizing the angular distribution of photoelectrons from the K-shell of N_2 [28]. Another consequence of this behaviour is that the sum of the contributions from the $1\sigma_g$ and $1\sigma_u$ shells shown in figure 7 does not display any interference modulation whatsoever at photoelectron momenta $k > 3$ au. Therefore it is crucially important to resolve the contributions of the $1\sigma_g$ and $1\sigma_u$ shells for observing the YDSE effect in molecules where these shells are filled. At lower momenta $k < 2.5$ au the σ^* shape resonance destroys the regular CF oscillations as is clearly displayed in figure 6.

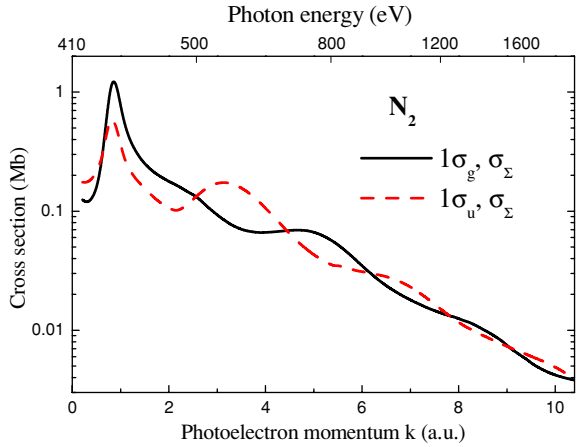

Figure 6. The total cross sections for the $\sigma \rightarrow \sigma$ transitions, σ_Σ, for the $1\sigma_g$ and $1\sigma_u$ shells calculated in the RPA (at $k \leqslant 3$ au) and the RCHF (at $k > 3$ au) approximation.

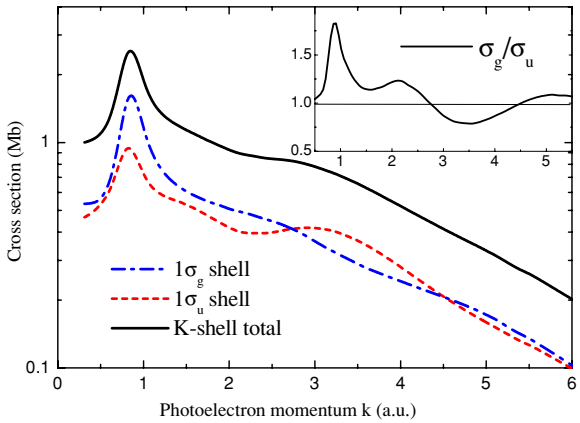

Figure 7. The partial photoionization cross sections for the $1\sigma_g$ and $1\sigma_u$ shells, and the total cross section for the K-shell of N_2 calculated in the RPA (at $k \leqslant 3$ au) and the RCHF (at $k > 3$ au) approximation. In the inset the ratio of the cross sections for the $1\sigma_g$ and $1\sigma_u$ shells is shown.

4. Analysis based on multiple scattering theory

4.1. Cohen–Fano two-centre interference

Let us turn our attention to the high energy region, where both the experimental and *ab initio* calculations show clearly the CF interference pattern. To give insights into the physics, we will investigate the high energy asymptotic of the wavefunction of the fast photoelectron. For that, it is reasonable to begin with the plane wave approximation that gives us immediately the CF formula. The CF result is a key reference point in our theory. The plane wave approximation will be improved in the next subsection, taking into account the scattering of the photoelectron by surrounding atoms.

When the homonuclear diatomic molecule is shined by an x-ray photon it is core-ionized from the well-defined quantum state

$$1\sigma_{g,u} = \frac{1s_1 \pm 1s_2}{\sqrt{2}}, \tag{13}$$

which is a coherent superposition of 1s levels (holes), localized in different atoms with coordinates $\mathbf{R}_1$ and $\mathbf{R}_2$. In such a Young's double-slit experiment, the two atoms in a homonuclear diatomic molecule play the role of slits which emit coherently phase shifted electronic waves $\propto \exp(\imath\mathbf{k}\cdot\mathbf{R}_1)$ and $\propto \exp(\imath\mathbf{k}\cdot\mathbf{R}_2)$. When an electron with momentum $\mathbf{k}$ is ejected from delocalized coherent gerade and ungerade core electron states (13), the interference of waves emitted coherently from indistinguishable atoms (holes) leads to an intrinsic YDSE interference pattern in the cross section of the K-shell photoinization

$$\sigma_{g,u}(\omega) \propto \tfrac{1}{2}|e^{\imath\mathbf{k}\cdot\mathbf{R}_1} \pm e^{\imath\mathbf{k}\cdot\mathbf{R}_2}|^2 = 1 \pm \cos(\mathbf{k}\cdot\mathbf{R}), \tag{14}$$

which depends on the parity of the core orbital, $\mathbf{k}$ and internuclear radius vector $\mathbf{R} = \mathbf{R}_1 - \mathbf{R}_2$. Molecules are randomly oriented in gas phase. The orientational averaging of the cross section (14) results in the Cohen–Fano interference pattern [1]

$$\sigma_{g,u}(\omega) = \sigma^{(0)}_{g,u}(\omega)\,(1 \pm \chi_{CF}(k))\,, \qquad \chi_{CF}(k) = \frac{\sin kR}{kR}, \qquad kR \gg 1 \tag{15}$$

where the cross section of the photoionization of a single atom $\sigma^{(0)}_{g,u}(\omega) \propto (\mathbf{e}\cdot\mathbf{k})^2$ by an x-ray photon with the polarization vector $\mathbf{e}$ is different in general for $1\sigma_g$ and $1\sigma_u$ shells, except in the high energy region where $\sigma^{(0)}_g(\omega) \approx \sigma^{(0)}_u(\omega)$.

From equation (15), the $\sigma_g(\omega)/\sigma_u(\omega)$ ratio can be given by

$$\frac{\sigma_g(\omega)}{\sigma_u(\omega)} = \gamma\frac{1 + \chi_{CF}(k)}{1 - \chi_{CF}(k)}, \tag{16}$$

where $\gamma = \sigma^{(0)}_g(\omega)\big/\sigma^{(0)}_u(\omega)$ and χ_{CF} is given by equation (15). It is worth noting that $\gamma \approx 1$ in the high energy region $kR \gg 1$.

The dash-dotted line in figure 2 is the interference pattern calculated by equation (16). Apparently, the phase of the interference pattern is shifted from both the experimental and *ab initio* ones. We note also that the CF formula neglects the nuclear motion. In other words, the internuclear distance between the two atoms is fixed. The experimental and *ab initio* interference patterns in the cross section ratio $\sigma_g(\omega)/\sigma_u(\omega)$ are significantly different for $0 \to 0$ and $0 \to 1$ vibrational transitions, as seen in figure 2.

4.2. Multiple scattering theory

We shall now derive the expression for the photoionization cross section in the high energy region

$$kR \gg 1 \tag{17}$$

taking into account the scattering of an ejected electron by surrounding atoms. We use the multiple scattering (MS) theory in the muffin-tin (MT) approximation [35]. This technique is nicely suited for fast electrons because the fast electron feels only an atomic core with the size k^{-1} times smaller than the atomic radius. In other words, the MS theory in the MT approximation becomes strict in the limit (17). To get the photoionization cross section

$$\sigma_{g,u}(\omega) \propto |\langle 1\sigma_{g,u}|\mathbf{e}\cdot\mathbf{r}|\psi_{\mathbf{k}}\rangle|^2, \tag{18}$$

we need wave $\psi_{\mathbf{k}}$ inside the muffin-tin (MT) sphere of the n (= 1, 2) th atom

$$\psi_{\mathbf{k}}(\mathbf{r}) = \sum_{lm} R_l(E, r_n)Y^*_{lm}(\hat{\mathbf{r}}_n)B^{(n)}_{lm}, \quad n = 1, 2, \tag{19}$$

where $R_l(E, r_n)$ is the radial wavefunction inside of the MT sphere, $\mathbf{r}_n = \mathbf{r} - \mathbf{R}_n$ is the electronic coordinate relative to the coordinate of the nth atom, $\mathbf{R}_n$, the spherical function $Y_{lm}(\hat{\mathbf{r}}_n)$ depends on the unit vector $\hat{\mathbf{r}}_n = \mathbf{r}_n/r_n$. According to equation (19) the cross section $\left|\sum_m e_m\left(B_{1m}^{(1)} \pm B_{1m}^{(2)}\right)\right|^2$ is the sum of two one-centre contributions and of the interference term

$$\sigma_{\mathrm{g,u}}(\omega) \propto |d(\omega)|^2 \left[\left|\sum_m e_m B_{1m}^{(1)}\right|^2 + \left|\sum_m e_m B_{1m}^{(2)}\right|^2 \pm 2\,\mathrm{Re}\sum_{mm_1} e_m B_{1m}^{(1)} e_{m_1}^* B_{1m_1}^{(2)*}\right], \tag{20}$$

where $d(\omega)$ is the transition dipole moment of atomic photoionization. Wave $B_{1m}^{(n)}$ incident on the nth MT sphere consists of the plane wave harmonic and the wave scattered by the n' atom towards atom n,

$$B_{lm}^{(n)} = 4\pi\imath^l\left[Y_{lm}(\mathbf{k})\,\mathrm{e}^{\imath\mathbf{k}\cdot\mathbf{R}_n} + \frac{\mathrm{e}^{\imath kR}}{R}Y_{lm}(\hat{\mathbf{R}}_{nn'})F_{nn'}\right], \qquad n' \neq n. \tag{21}$$

Here $\mathbf{R}_{nn'} = \mathbf{R}_n - \mathbf{R}_{n'}$, $R = R_{21}$. In the high energy limit, the effective amplitude of electron scattering from the n' th atom towards the nth atom of a diatomic molecule obeys multiple scattering (MS) equation [36]

$$F_{nn'} = f^{(n')}(\theta[\mathbf{R}_{nn'}, \mathbf{k}])\,\mathrm{e}^{\imath\mathbf{k}\cdot\mathbf{R}_{n'}} + f^{(n')}(\pi)\frac{\mathrm{e}^{\imath kR}}{R}F_{n'n}, \tag{22}$$

where $\theta[\mathbf{k}_1, \mathbf{k}]$ is the angle between $\mathbf{k}_1$ and $\mathbf{k}$. The partial scattering amplitudes $f_l^{(n)}$ with the scattering phase δ_l^n form the total amplitude of electron scattering by the nth atom according to the Faxén–Holtsmark formula [37]

$$f^{(n)}(\hat{\mathbf{k}}'\cdot\hat{\mathbf{k}}) = 4\pi\sum_{lm} f_l^{(n)} Y_{lm}^*(\mathbf{k}')Y_{lm}(\mathbf{k}), \qquad f_l^{(n)} = \frac{\mathrm{e}^{2\imath\delta_l^n} - 1}{2\imath k}. \tag{23}$$

Multiple scattering equations (22) can be solved explicitly to give

$$F_{nn'} = \frac{1}{\kappa}\left\{f^{(n')}(\theta[\mathbf{R}_{nn'}, \mathbf{k}])\,\mathrm{e}^{\imath\mathbf{k}\cdot\mathbf{R}_{n'}} + f^{(n')}(\pi)\frac{\mathrm{e}^{\imath kR}}{R}f^{(n)}(\theta[\mathbf{R}_{n'n}, \mathbf{k}])\,\mathrm{e}^{\imath\mathbf{k}\cdot\mathbf{R}_n}\right\}, \quad n' \neq n. \tag{24}$$

where

$$\kappa = 1 - f^{(1)}(\pi)f^{(2)}(\pi)\frac{\mathrm{e}^{2\imath kR}}{R^2}. \tag{25}$$

In the high energy region the backscattering amplitude is small compared with bond length, $(|f(\pi)|/R)^2 \ll 1$. This means that

$$\kappa \approx 1. \tag{26}$$

Due to this, only scattering events up to double scattering contribute to amplitude $B_{lm}^{(n)}$ (see figure 8):

$$B_{lm}^{(n)} = 4\pi\imath^l\left[\mathrm{e}^{\imath\mathbf{k}\cdot\mathbf{R}_n}\left\{Y_{lm}(\hat{\mathbf{k}}) + \frac{\mathrm{e}^{2\imath kR}}{R^2}Y_{lm}(\hat{\mathbf{R}}_{nn'})f^{(n')}(\pi)f^{(n)}(\theta[\mathbf{R}_{n'n}\cdot\mathbf{k}])\right\}\right.$$
$$\left. + \frac{\mathrm{e}^{\imath kR}}{R}Y_{lm}(\hat{\mathbf{R}}_{nn'})f^{(n')}(\theta[\mathbf{R}_{nn'}\cdot\mathbf{k}])\,\mathrm{e}^{\imath\mathbf{k}\cdot\mathbf{R}_{n'}}\right], \qquad n' \neq n. \tag{27}$$

The substitution of this result into equation (20) gives immediately the cross section of photoionization of fixed-in-space molecules. However, this expression is rather lengthy. Due to this we will go directly to our main goal: the photoionization of randomly oriented molecules.

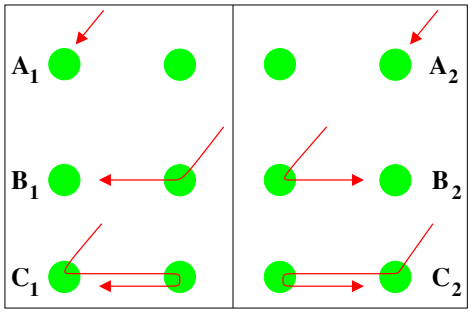

Figure 8. (A_n) No scattering. (B_n) Single scattering. (C_n) Double scattering. One-centre photoionization: $|A_n + B_n + C_n|^2$. The two-centre interference: $\mathrm{Re}\{(A_1 + B_1 + C_1)(A_2 + B_2 + C_2)^*\}$.

4.3. Photoionization of randomly oriented molecules

Let us now focus our attention on the important case of randomly oriented molecules. Before writing down the expression for the cross section (see equations (20) and (27)) averaged over molecular orientations, we would like to mention some important points used in such an averaging. First of all, we use the stationary phase approximation

$$\int \mathrm{d}\hat{\mathbf{R}}\, \mathrm{e}^{\imath \mathbf{k}\cdot\mathbf{R}} \Phi(\hat{\mathbf{R}}) = \frac{2\pi}{\imath kR}(\mathrm{e}^{\imath kR}\Phi(\hat{\mathbf{k}}) - \mathrm{e}^{-\imath kR}\Phi(-\hat{\mathbf{k}})) + O\left(\frac{1}{(kR)^2}\right), \tag{28}$$

and the Faxén–Holtsmark partial wave expansion of the atomic scattering amplitude (23). During averaging procedure the forward scattering amplitude, $\mathrm{Im}\, f(0)$, appears. This first-order term is cancelled by the second-order contribution due to the optical theorem

$$\frac{4\pi}{k}\,\mathrm{Im}\, f(0) = \int \mathrm{d}\hat{\mathbf{k}} |f(\theta)|^2\, \mathrm{d}\theta. \tag{29}$$

We also skip the index of the atom ($f^{(n)}(\theta) \to f(\theta)$, $\delta_1^{(n)} \to \delta_1$), due to the symmetry of the molecule.

So the averaging over $\hat{\mathbf{R}}$ results in the following formula for the photoionization cross section,

$$\sigma_{\mathrm{g,u}}(\omega) = 3\sigma_0(\omega)\left[(\mathbf{e}\cdot\mathbf{k})^2\left(1 - \frac{1}{kR^2}\,\mathrm{Im}(f(\pi)\,\mathrm{e}^{\imath 2(kR+\delta_1)})\right)\right.$$
$$\left. + \frac{1}{2}(1 - 3(\mathbf{e}\cdot\mathbf{k})^2)\frac{\sigma_{\mathrm{tr}}(k)}{4\pi R^2} \pm \frac{(\mathbf{e}\cdot\mathbf{k})^2}{kR}\sin(kR + 2\delta_1)\right], \tag{30}$$

where the terms up to the second order over the scattering amplitude, $f(\theta)$, are taken into account. Here we introduced the transport cross section related to the viscosity coefficient

$$\sigma_{\mathrm{tr}}(k) = 2\pi \int_0^\pi |f(\theta)|^2 \sin^3\theta\, \mathrm{d}\theta, \tag{31}$$

which is usually small compared with the total cross section of electronic scattering. The second term in equation (30) is quenched when the photoelectrons are collected from the entire solid angle, 4π.

The first two terms on the right-hand side of equation (30) arise from the first two terms in equation (20) and they describe one-centre photoionization of two atoms. The last term in equation (30), similar to the CF formula (15), describes the two-centre interference of

indistinguishable ionization channels. The scattering correction for the one-centre contribution is small, because in the high energy region (17)

$$\frac{|f(\pi)|}{R} \ll 1, \qquad \frac{\sigma_{\rm tr}(k)}{R^2} \ll 1. \tag{32}$$

So, finally, the photoionization cross section turns out to be surprisingly simple,

$$\sigma_{\rm g,u}(\omega) = \sigma^{(0)}_{\rm g,u}(\omega)\,(1 \pm \chi(k))\,. \tag{33}$$

This equation coincides with the CF formula (15) except the interference factor

$$\chi(k) = \frac{\sin(kR + 2\delta_1)}{kR}, \tag{34}$$

which shows that the electron scattering shifts the CF interference pattern (15). The physical origin of this phase shift is the two-centre interference of the free wave (A_1) and single scattered wave (B_2) shown in figure 8.

We have arrived at our key results: the electron scattering that is negligibly small in the one-centre term photoionization of (30) is enhanced anomalously due to the two-centre or YDSE interference. Indeed, contrary to the small scattering amplitude (32), phase δ_1 is large and strongly depends on k in the entire range of the photoelectron energies.

We apply equations (33) and (34) to the nitrogen molecule N_2. Both gerade and ungerade core levels are occupied in N_2. Due to this, in the x-ray photoionization profile of nitrogen the core shell consists of two spectral lines $1\sigma_{\rm g} \to \psi_{\mathbf{k}}$ and $1\sigma_{\rm u} \to \psi_{\mathbf{k}}$ with the relative intensities

$$\frac{\sigma_{\rm g}(\omega)}{\sigma_{\rm u}(\omega)} = \gamma\,\frac{1+\chi(k)}{1-\chi(k)}. \tag{35}$$

4.4. Determination of the scattering phase

To compare the experimental data with the theory (equations (34) and (35)), we use the following approach. We first take the sum over the vibrational components for the experimental spectra and obtain the ratios as shown in figure 9. Following Teo and Lee [31], we use a quadratic approximation for the phase shift:

$$2\delta_1 = a + bk + ck^2. \tag{36}$$

One can estimate values $a = -4.8$, $b = -1.15$ and $c = 0.069$ au via interpolation of *ab initio* estimates for the scattering phases $2\delta_1(k)$ for C and O [31]. γ in equation (35) can be assumed to be 1. The resulting cross section ratio is shown in figure 9 by the dash-dotted line. The agreement with the experiment is improved in comparison with the original Cohen–Fano approach but it is still far from being fair.

We can obtain the improved value of the scattering phase $2\delta_1(k)$ using a least-squares fitting of equations (34) and (35) to the experimental ratios as shown in figure 9, regarding a, b and c in equation (36) as fitting parameters. The resulting values via the fitting are $a = -5.2 \pm 0.6$, $b = -1.6 \pm 0.4$, $c = 0.09 \pm 0.05$ au. The fitting also results in $\gamma = 1.04 \pm 0.04$, in reasonable agreement with the expected value $\gamma = 1$. This result is shown in figure 9 by the solid line. Now the agreement with the experiment is rather good. Since this method describes only the high energy region, the variation of the cross section ratio at low photoelectron momenta below 2 au governed by the shape resonance is not reproduced in this theory.

For comparison, we show in figure 9 also the RPA result without the vibrational resolution which corresponds to the sum of two vibrational transitions shown separately in figure 2. The RPA result is in a reasonable agreement with the experiment at all photoelectron momenta studied.

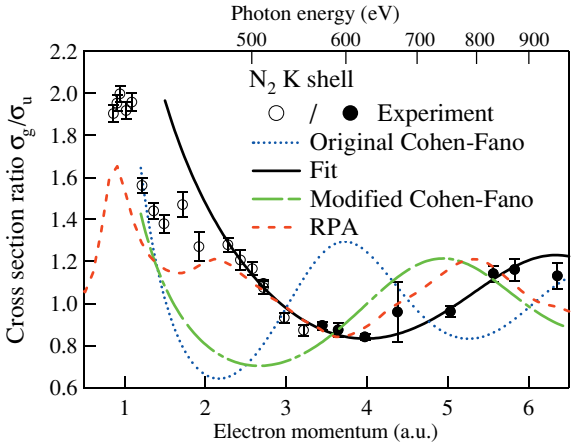

Figure 9. Ratios of $1\sigma_g$ and $1\sigma_u$ partial photoionization cross sections of N_2 summed over the vibrational components. Open and full circles—previous [11–13] and present experiments, respectively. Dotted line—the Cohen–Fano formula; dash-dotted line—the present modified Cohen–Fano formula with *ab initio* scattering phase; solid line—fitted curve by the present modified Cohen–Fano formula regarding the scattering phase as a fitting function; dashed line—the RPA calculation. See the text for further details.

5. Conclusion

We studied experimentally and theoretically the interference modulation in the vibrationally resolved photoelectron spectra of the $1\sigma_g$ and $1\sigma_u$ shells of the N_2 molecule in the photon energy range from the threshold up to 1 keV. We demonstrated that the ratios of the $1\sigma_g$ to $1\sigma_u$ photoionization cross sections display the interference modulation that is caused by coherent photoemission from the two N atoms and is an analogue of Young's double-slit experiment. The calculations in the random phase approximation (section 3) reproduce the experimental data reasonably well. A detailed analysis of the partial cross sections in RPA has been performed neglecting the vibrational splitting. This analysis showed that the modulation is connected with the onset of transitions to the states of increasing orbital angular momentum which occurs at increasing photon energies as was mentioned by Cohen and Fano [1]. Evidently, the interference phenomena in the N_2 molecule, due to the presence of two K-shells of different symmetry, gerade and ungerade, are more complex as compared to the case of the H_2 molecule considered originally in [1]. We demonstrated that the interference modulations for the $1\sigma_g$ and $1\sigma_u$ shells are in antiphase. It is explained by the dipole selection rules according to which only odd and even partial waves contribute to the photoionization from the gerade and ungerade K-shells, respectively. The calculations also demonstrate that the main contribution to these modulations comes from the $\sigma \rightarrow \sigma$ transitions. The coherence between the two waves originating from two different N atoms breaks down when the spectral resolution is not sufficient to resolve the gerade and ungerade doublet. In other words, the photoionization cross section does not display any interference pattern when the spectral resolution is not sufficient.

Another important point is that both our experimental and *ab initio* calculations display considerable deviation from the Cohen–Fano formula. To explain this disagreement, we derived an analytical formula for the interference pattern in the high energy region using multiple scattering theory (section 4). We show that the Cohen–Fano interference pattern is

shifted by twice the phase of the photoelectron scattering by the neighbouring N atom. The newly obtained formula for the interference pattern is in a good agreement with the results of our experiments at high energies. An interesting point is that the electron scattering that is negligibly small in the one-centre term photoionization is enhanced anomalously due to the two-centre interference. The shift of the Cohen–Fano interference pattern gives a new opportunity to measure directly the scattering phase of the photoelectron, which is needed in different applications, for example, in the EXAFS studies of the molecular structure.

Acknowledgments

The experiment was carried out with the approval of the SPring-8 program review committee and supported in part by grants-in-aid for scientific research provided by the Japan Society for Promotion of Science (JSPS). The authors thank the staff at SPring-8 for their help during the experiment. NAC and FG are grateful to Tohoku University for hospitality and financial support during their stay in Japan. NAC and SKS acknowledge financial support from the INTAS. VK and FG acknowledge support from the Swedish Research council (VR) and the STINT foundation. XJL and TL are grateful to the COE program at Tohoku University and JSPS for financial support.

References

[1] Cohen H D and Fano U 1966 *Phys. Rev.* **150** 30
[2] Kaplan I G and Markin A P 1969 *Sov. Phys. Dokl.* **14** 36
[3] Walter M and Briggs J 1999 *J. Phys. B: At. Mol. Opt. Phys.* **32** 2487
[4] Fojón O A, Fernándes J, Palacios A, Rivarola R D and Martin F 2004 *J. Phys. B: At. Mol. Opt. Phys.* **37** 3035
[5] Fojón O A, Palacios A, Fernándes J, Rivarola R D and Martin F 2006 *Phys. Lett.* A **350** 371
[6] Misra D, Kadhane U, Singh Y P, Tribedi L C, Fainstein P D and Richard P 2004 *Phys. Rev. Lett.* **92** 153201
[7] Hossain S, Alnaser A S, Landers A L, Pole D J, Knutson H, Robison A, Stamper B, Stolterfoht N and Tanis J A 2003 *Nucl. Instrum. Methods Phys. Res.* B **205** 484
[8] Kamalou O, Chesnel J-Y, Martina D, Hanssen J, Stia C R, Fojón O A, Rivarola R D and Frémont F 2005 *Phys. Rev.* A **71** 010702
[9] Rolles D *et al* 2005 *Nature* **437** 711
[10] Hergenhahn U, Kugeler O, Rüdel A, Rennie E E and Bradshaw A M 2001 *J. Phys. Chem.* A **105** 5704
[11] Semenov S K *et al* 2006 *J. Phys. B: At. Mol. Opt. Phys.* **39** 375
[12] Ehara M *et al* 2006 *J. Chem. Phys.* **124** 124311
[13] Semenov S K *et al* 2006 *J. Phys. B: At. Mol. Opt. Phys.* **39** L261
[14] Kukk E *et al* 2005 *Phys. Rev. Lett.* **95** 133001
[15] Ohashi H *et al* 2001 *Nucl. Instrum. Methods* A **467–468** 529
[16] Ohashi H *et al* 2001 *Nucl. Instrum. Methods* A **467–468** 533
[17] Tanaka T and Kitamura H 1996 *J. Synchrotron Radiat.* **3** 47
[18] Shimizu Y *et al* 2001 *J. Electron Spectrosc. Relat. Phenom.* **63** 114
[19] Semenov S K, Cherepkov N A, Fecher G H and Schönhense G 2000 *Phys. Rev.* A **61** 032704
[20] Semenov S K and Cherepkov N A 2002 *Phys. Rev.* A **66** 022708
[21] Lynch D L and McKoy V 1984 *Phys. Rev.* A **30** 1561
[22] Semenov S K, Cherepkov N A, Jahnke T and Dörner R 2004 *J. Phys. B: At. Mol. Opt. Phys.* **37** 1331
[23] Dill D and Dehmer J L 1974 *J. Chem. Phys.* **61** 692
[24] Amusia M Ya and Cherepkov N A 1975 *Case Studies At. Phys.* **5** 47
[25] Hergenhahn U 2004 *J. Phys. B: At. Mol. Opt. Phys.* **37** R89
[26] Semenov S K, Cherepkov N A, De Fanis A, Tamenori Y, Kitajima M, Tanaka H and Ueda K 2004 *Phys. Rev.* A **70** 052504
[27] Thiel A, Schirmer J and Köppel H 2003 *J. Chem. Phys.* **119** 2088
[28] Hosaka K, Adachi J, Golovin A V, Takahashi M, Teramoto T, Watanabe N, Yagishita A, Semenov S K and Cherepkov N A 2006 *J. Phys. B: At. Mol. Opt. Phys.* **39** L25
[29] Gel'mukhanov F, Carravetta V and Ågren H 1998 *Phys. Rev.* B **58** 2216

[30] Lee P A, Citrin P H, Eisenberger P and Kincaid B M 1981 *Rev. Mod. Phys.* **53** 769
[31] Teo B-K and Lee P A 1979 *J. Am. Chem. Soc.* **101** 2815
[32] Domcke W and Cederbaum L S 1978 *Chem. Phys. Lett.* **13** 161
[33] Gel'mukhanov F, Sałek P and Ågren H 2001 *Phys. Rev.* A **64** 012504
[34] Felicíssimo V C, Guimarães F F and Gel'mukhanov F 2005 *Phys. Rev.* A **72** 023414
[35] Stöhr J 1992 *NEXAFS Spectroscopy* (Berlin: Springer)
[36] Gel'mukhanov F, Carravetta V and Ågren H 1998 *Phys. Rev.* B **58** 2216
[37] Mott N F and Massey H S W 1933 *The Theory of Atomic Collisions* (London: Oxford University Press)
[38] Gel'mukhanov F and Ågren H 1994 *Phys. Rev.* A **49** 4378
[39] Mills J D, Sheehy J A, Ferrett T A, Southworth S H, Mayer R, Lindle D W and Langhoff P W 1997 *Phys. Rev. Lett.* **79** 383
[40] Gel'mukhanov F and Ågren H 1999 *Phys. Rep.* **312** 91
[41] Kempgens B, Köppel H, Kivimäki A, Neeb M, Cederbaum L S and Bradshaw A M 1997 *Phys. Rev. Lett.* **79** 3617